Evaluation of a Clinical Scintillation Camera with Pulse Tail Extrapolation Electronics

Thomas K. Lewellen, Alden N. Bice, Kenneth R. Pollard, Jia-Bi Zhu, and Marianne E. Plunkett

Division of Nuclear Medicine, Department of Radiology, University of Washington, Seattle, Washington

The performance of a new scintillation camera, designed for high event rate capability, was evaluated. The system consisted of a 400 mm field-of-view NaI(T1) camera with 61 photomultiplier tubes and modified General Electric Starport electronics. A significant feature of the system was circuitry for performing pulse tail extrapolation and separation of individual pulses involved in pulse pile-up events. System deadtime, flood field uniformity, energy resolution, linearity, spatial resolution, and bar phantom image quality were evaluated for count rates up to 200 kcps in a 20% photopeak window. Our results indicate that this camera design does not compromise image quality at normal clinical count rates and at higher event rates can provide better image quality and increased sensitivity over many Anger cameras currently employed in nuclear medicine.

J Nucl Med 30:1554–1558, 1989

Anger cameras, like other radiation detectors, suffer the effects of pulse pile-up. During high-count-rate studies, pulse pile-up is responsible for increased camera deadtime losses and image distortion with loss of image contrast and detail. A continuing goal of camera designers has been to provide high-counting-rate capability with minimal deadtime losses and acceptable image quality (i.e., minimum misplaced counts, loss of spatial and energy resolution, and loss of uniformity).

A basic problem during high-counting-rate studies is the response of the amplifier that shapes each of the preamplifier pulses (*1–4*). In most gamma cameras, there is a set of amplifiers that integrates the detector pulses to produce a shaped output pulse whose height is proportional to the amount of energy deposited by the scintillation crystal. Nuclear medicine textbooks usually discuss this integrator in terms of a single-channel-spectroscopy linear amplifier system, but the basic principles apply to any part of the imaging system electronics that integrate and shape pulses. The input signals to these integrators may be relatively long tailed pulses. Ideally, the entire preamplifier pulse should be integrated in order to obtain the best measurement of the event's energy. However, a long integration time increases the probability that two (or more) events will be integrated together (pulse pile-up) to produce a single, distorted output pulse (Fig. 1A). These distorted output pulses are used in the subsequent signal processing of the camera.

One commonly implemented method for pulse pile-up reduction is to have the integrator process only the first part of the pulse. This strategy diminishes the effects of the succeeding pulses but degrades energy and spatial resolution (*1–5*). Pulse pile-up is not eliminated, but higher counting rates are required before it is prominent. A second commonly implemented method for pile-up rejection is to start a timer when the integrator output pulse rises above a very low voltage level (*3*). If the output pulse does not return close to its baseline value by a preset time, then the pulse is considered distorted and is rejected. With this method increasing numbers of events are discarded at increasing event rates.

Another problem of the amplifier system at high counting rates is baseline shift. Baseline shift is usually corrected in scintillation cameras using pole zero cancellation or baseline restoration (*1–3*). If the compensation is not adequate, shifts in peak energy positions and image location can result.

In all of these approaches, little is really done to adjust for the voltage pedestal under a pulse caused by a preceding pulse's tail. An integration and shaping circuit that could also address the pedestal and pile-up

Received Dec. 12, 1988; revision accepted Apr. 25, 1989.

For reprints contact: Thomas K. Lewellen, PhD, Dept. of Radiology, RC-05, University Hospital, Seattle, WA 98195.

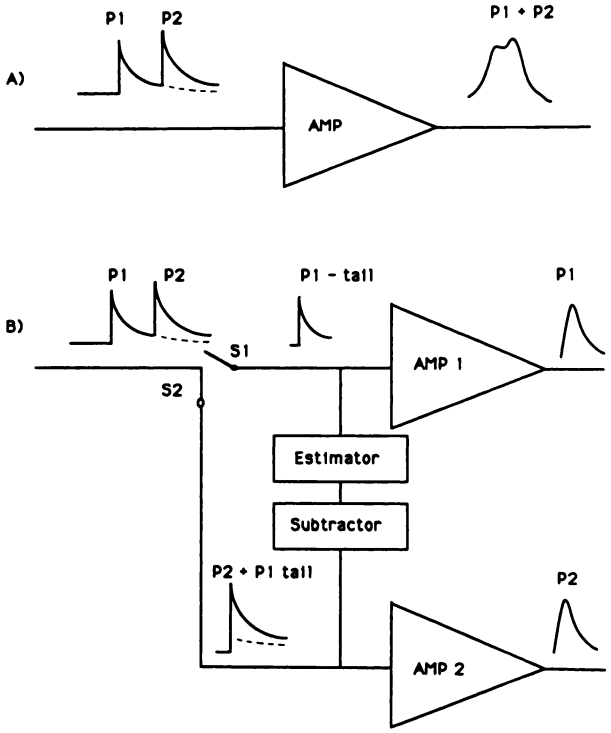

FIGURE 1
Normal pulse pile-up and the basic pulse tail extrapolation system. Part A depicts the single distorted output pulse from the amplifier that results when two analog pulses arrive too close together in time. Part B depicts the pulse tail extrapolation system designed to correct for pulse pile-up (explained in the text).

problems would be of interest in scintillation camera design. This paper presents initial test results of a prototype scintillation camera developed by General Electric Medical Systems that uses a technique known as pulse tail extrapolation to achieve high count rate performance while maintaining good image quality.

MATERIALS AND METHODS

Pulse Tail Extrapolation

The basic technique of pulse tail extrapolation is indicated in Figure 1. The pulse tail extrapolation circuit monitors the incoming pulse to the amplifier and follows the decay of the pulse tail with a circuit termed an estimator. If the input to the estimator is opened (the incoming pulse is disconnected from the estimator), then the estimator produces an output that approximates the remainder of the pulse, using the known decay constants for the instrument. These estimator circuits can then be used as diagrammed in Figure 1B. A pulse (P1) is first routed to channel 1. A set of fast leading edge discriminators monitors the incoming signal, and if a second pulse (P2) occurs before the first pulse has returned to baseline, the input to channel 1's amplifier is disconnected and the second signal (i.e., sum of P2 and P1's tail) is connected to channel 2. The estimator now supplies an estimate of P1's tail to the first amplifier. The output of the estimator is also routed to channel 2's amplifier. The estimated tail of the first pulse (P1) is subtracted from the current signal being presented to the second amplifier.

In this way, the first pulse is amplified and shaped in circuit number one without any distortion from the second pulse, and the second pulse is corrected for the pedestal from the first pulse. If a third pulse occurs before the second pulse has returned to base line, the process is repeated with a third amplifier/estimator circuit. In this case the estimated pulse tails of the first two pulses are subtracted from the third pulse. The net result of the circuitry is a better estimate of each of the overlapping pulse's shape. Fewer events are lost and the output signals have less distortion.

Count rate tests were performed on a prototype for a new digital scintillation camera (model 400HPC) (The production model name is Starcom 3000 XC/T) designed and built by General Electric Medical Systems and installed in our clinical laboratory. The system consisted of a 400-mm field-of-view NaI(Tl) camera with 61 photomultiplier tubes and a modified Starport electronics system for camera control and data acquisition. Included in the normal operating mode of the camera are lookup correction tables for energy variation with position, and x and y spatial linearity variations.

The system tested had five levels of pulse tail extrapolation, allowing compensation for pile-up of up to four pulses after the first pulse is detected.

Count Rate Tests

Observed versus true count rate curves were measured for the 400HPC using the decaying source method. A small glass vial containing technetium-99m (^{99m}Tc) activity (2 cm^3 fluid volume) was fixed ~2 m in front of the uncovered camera crystal. No scattering medium was employed. Counts per second (cps) recorded in a 256 × 256 image matrix were measured at regular time intervals over a period of 32 hr as the source decayed. Four energy windows were investigated; a wide open window (~0–500 keV), a symmetric 20% photopeak window and two asymmetric 10% windows, one centered 5% above the photopeak energy, the other centered 5% below the photopeak energy. The last count rate measurement was taken when the ^{99m}Tc activity had decayed enough to produce a counting rate of 13 800 cps in the full-energy spectrum. This lowest count rate measurement was assumed to be free of data loss (The assumption of no data loss at 13 800 cps in the full energy spectrum introduces no more than a 1.5% underestimation of the true counting rate) (i.e., no deadtime or pulse pile-up) and was used to calculate the true camera counting rates at the higher ^{99m}Tc activities. Energy and spatial linearity correction systems were active during the measurements.

Flood Uniformity

Flood images for the prototype camera were obtained by placing a small ^{99m}Tc source 2 m away from the uncollimated detector head. A lead ring was placed on the camera to define a 37-cm useful field of view (UFOV). Using a symmetric 20% photopeak window, images at seven counting rates were obtained: 200 000 cps (200 kcps), 150 kcps, 100 kcps, 75 kcps, 50 kcps, 25 kcps, and <10 kcps. A 128 × 128 pixel array was used to acquire images containing 2 × 10^7 events. Flood field uniformity was calculated as recommended in the National Electrical Manufacturers Association (NEMA) standards (*6*).

Energy and spatial linearity correction systems were active during the measurements.

Energy Resolution

System intrinsic energy resolution was measured as the FWHM of the photopeak as recommended by the NEMA standards. Intrinsic energy resolution also was measured at higher counting rates, 200 kcps, 150 kcps, 100 kcps, 75 kcps, 50 kcps, 25 kcps (as defined by a 20% symmetric photopeak window). Energy and spatial linearity correction systems were active during the measurements.

Linearity and Spatial Resolution

A NEMA linearity phantom was used to acquire 5×10^6 count linearity images for the camera X and Y directions. The observed counting rate in the 20% energy window was 9 kcps during the acquisitions. System energy and spatial linearity correction tables were employed. Total system linearity and spatial resolution were calculated as recommended in the NEMA standards. The energy and spatial linearity correction systems were active during the measurements.

Bar Phantom Images

Bar phantom images with 2×10^7 events were acquired in 256×256 pixel arrays using a ^{99m}Tc source located 2 m away from the detector head. The phantom had 4 mm, 3 mm, 2.5 mm, and 2 mm thick lead bars which were separated by a distance equal to their thickness, respectively. A symmetric 20% photopeak window was used in the acquisitions. Images with 100 kcps, 75 kcps, 50 kcps and <10 kcps in the energy window were acquired. Energy and spatial linearity correction systems were active during the measurements.

RESULTS

Figure 2 presents graphs of the observed counting rate versus the true counting rate of the 400HPC camera for the four energy windows investigated. Over the range of event rates commonly encountered in the nuclear medicine clinic the 400HPC camera had data losses that were <5% for a 20% window. The 20% count rate loss (in a 20% window, Fig. 2B) occurred at an observed count rate of 170 kcps when measured with the decaying source method. The maximum observable count rate in a 20% window was not obtained in our measurements. It was in excess of 230 kcps. At an incident count rate of 590 kcps, the 400HPC system appears to have reached its maximum counting rate of 420 kcps (wide open window, Fig. 2A).

Figures 2C and 2D show the count rate curves for 10% energy windows located 5% above and below the photopeak, respectively. The 10% window that is above the photopeak shows a slightly higher count rate performance then the other 10% window, reflecting a slight asymmetry in photopeak shape.

Table 1 lists the measured differential and integral flood field uniformity for the 400HPC at various counting rates. Uniformity data are given for the useful field of view (UFOV) and the central field of view (CFOV).

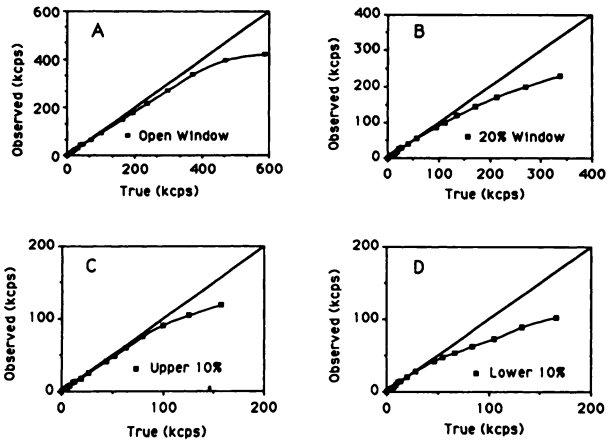

FIGURE 2
Plots of observed versus true counts within the pulse height analyzer (PHA) window of the pulse tail extrapolation system (GE 400HPC scintillation camera). Part A is for a 100% pulse height analyzer (PHA) window. Part B is a 20% symmetric PHA window centered on the ^{99m}Tc photopeak. Part C is for a 10% PHA window with the centerline shifted up in energy by 5% from the photopeak value. Part D is a 10% PHA window with the centerline shifted down in energy by 5% from the photopeak value.

At count rates up to 100 kcps there is little change in the integral and differential uniformity values. Uniformity is degraded only slightly at 150 kcps and more noticeably at 200 kcps.

Table 1 also lists the measured intrinsic energy resolution at the various count rates for a 20% window. At low counting rates the camera energy resolution is below 10%. At 100 kcps the energy resolution is still only 10.8%.

TABLE 1
Flood Field Uniformity Values and Camera Intrinsic Energy Resolution Measured at Different Count Rates*

Count rate* (kcps)		Flood uniformity UFOV (%)	CFOV (%)	Energy resolution FWHM (%)
10	Diff	2.3	1.9	9.6
	Int	4.0	2.6	
25	Diff	1.8	1.8	9.7
	Int	3.9	2.6	
50	Diff	2.2	2.2	10.0
	Int	4.2	3.1	
75	Diff	2.4	2.2	10.3
	Int	4.0	3.3	
100	Diff	2.8	2.5	10.8
	Int	5.2	3.9	
150	Diff	3.4	2.7	11.6
	Int	6.7	4.5	
200	Diff	4.2	3.1	13.0
	Int	8.1	5.3	

*The count rate values refer to the observed count rate in a 20% window. Diff and Int refer to differential and integral, respectively.

Table 2 lists the measured intrinsic spatial resolution and the system linearity for the UFOV and CFOV. The intrinsic spatial resolution was found to be 3.6 mm in the UFOV. The absolute and differential linearities for the UFOV were 0.5 mm and 0.1 mm, respectively.

Figure 3 depicts a series of intrinsic flood images from the 400HPC with the same total number of events but acquired at different counting rates (20, 50, 100, and 200 kcps). At a count rate of 200 kcps there is some image degradation visible, consistent with the data in Table 1. Qualitatively, the image degradation is subtle.

Figure 4 shows a series of bar phantom images acquired with the 400HPC camera at four different event rates (<10, 50, 75, and 100 kcps). Qualitatively there is little difference in the four images. The 2.5-mm bars are easily resolved at the four counting rates.

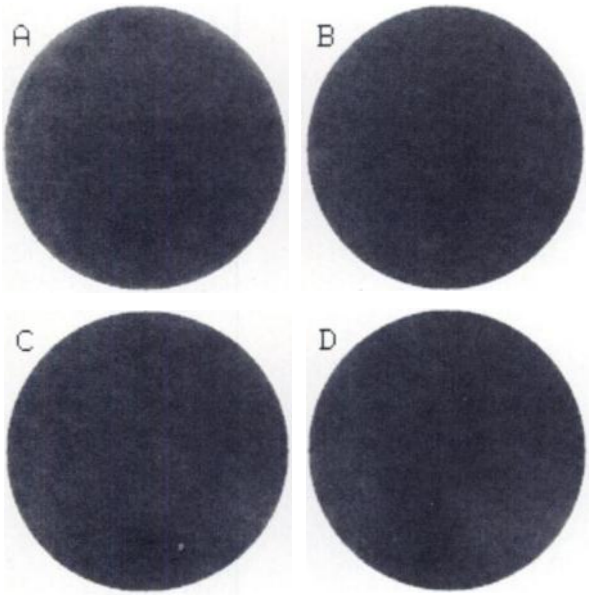

FIGURE 3
Intrinsic flood images acquired at different counting rates with the 400HPC camera. Each flood image contains 2×10^7 events in a 128 × 128 pixel array. Images A, B, C, and D were acquired at 200, 100, 50, and 20 kcps, respectively, within a 20% symmetric pulse height analyzer window centered on the ^{99m}Tc photopeak.

DISCUSSION

The count rate performance of Anger scintillation cameras has improved substantially over the years. Faster electronics and modified pulse shaping schemes have allowed the manufacture of cameras with count rate performance suitable for most imaging studies. However, even modern cameras suffer the effects of pulse pile-up at high count rates because of the finite scintillation decay time of NaI (~0.25 μsec, 3,4). Further improvements in camera counting performance would be possible if overlapping events could be "unpiled" by using the known time constants of the crystal and amplifiers to estimate the true shape of each event pulse. We evaluated the count rate performance of a new clinical scintillation camera (GE 400HPC) equipped with circuitry for estimating individual analog pulses that comprise a pile-up event.

Figures 2A, 2B, 2C, and 2D indicate the number of events recorded within four different energy windows on the prototype camera for total event rates up to nearly 600 kcps. The count rate for a 20% data loss was 170 kcps for the 400HPC. This may be compared with the 20% loss rate of ~65 kcps to 160 kcps for the GE 400A series of cameras (*7*) or other Anger camera systems (*8*).

Pulse estimation circuits can help overcome the pedestal offset effects from preceding pulse tails at high counting rates and thus preserve the intrinsic camera resolution over a greater counting range. The 400HPC camera has an energy resolution of 9.6%. At observed counting rates of 100 kcps in a 20% window the intrinsic energy resolution of the system has degraded slightly to 10.8%. This is still better than the NEMA energy resolution specified for many systems currently in use at low event rates.

Figures 2C and 2D indicate that at low counting rates (<50 kcps), the photopeak is symmetric. At higher counting rates there is a slight upward shift in the determination of photopeak event energy. At the highest counting rate measured, the lower 10% energy window had 14% fewer events than the upper 10% energy window. This difference may reflect the pulse tail extrapolation circuitry's ability to separate pile-up events, including slight inaccuracies in the extrapolation time constants. Further work would be required to assess the effects of this difference on very high count rate clinical studies that use an asymmetric photopeak energy window.

Figures 3 and 4 qualitatively demonstrate the stability of the 400HPC system uniformity and spatial resolution over and beyond the counting range normally encountered in the clinic. Table 1 indicates that flood field

TABLE 2
Absolute and Differential Linearity Values and the Intrinsic Spatial Resolution of the 400HPC Camera*

Total	UFOV*	CFOV*
Absolute	0.5 mm	0.3 mm
Differential	0.1 mm	0.1 mm
FWHM	3.6 mm	3.4 mm
FWTM	6.8 mm	6.6 mm

* UFOV and CFOV refer to the useful field of view and central field of view, respectively. FWHM and FWTM refer to full width at half maximum and full width at tenth maximum, respectively.

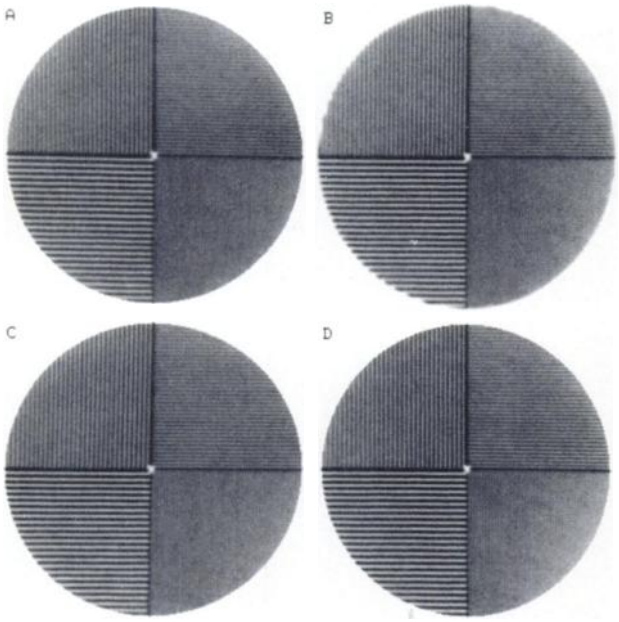

FIGURE 4
Bar phantom images containing 2×10^7 events in 256 × 256 pixel arrays obtained at different counting rates with the 400HPC camera. Image A, B, C, and D were acquired at 100, 75, 50 and <10 kcps, respectively, within a 20% symmetric pulse height analyzer window centered on the ^{99m}Tc photopeak. The phantom had 4-mm, 3-mm, 2.5-mm, and 2-mm wide lead bars which were separated by a distance equal to their width, respectively. Acquisition with a 512 × 512 matrix would yield higher resolution images than those shown.

uniformity remained quite good even at an observed count rate of 150 kcps in a 20% window. Because of the large amounts of activity required, it was not feasible to measure spatial linearity at high event rates. Figure 4 shows no evidence of linearity distortion at the higher event rates.

The present results were obtained using only ^{99m}Tc radioactivity and an absence of scattering medium. Whereas there is little reason to expect that the pulse-tail extrapolation circuitry would not perform well under other conditions, further evaluations of this camera design should include performance measurements over a range of primary photon energies (e.g., thallium-201 and gallium-67) and the presence of a scattering continuum. Indeed, patient studies performed in our clinic with ^{99m}Tc-labeled tracers demonstrated good performance of the 400HPC camera.

Given the availability of a scintillation camera with improved performance at high count rates, what would be its utility in the clinical setting? A few nuclear medicine centers would utilize the enhanced count rate performance when using very short-lived isotopes for high speed dynamic studies, such as first-pass studies of the heart (*9*). For the majority of clinical laboratories the primary benefit of a camera with pulse tail extrapolation would be in increased counting efficiency for normal clinical studies. In our clinic the cardiac studies currently have the highest counting rates, with rates between 40 kcps and 75 kcps common. With the prototype system, the percentage of lost counts at 75 000 events per second is less than a few percent as compared to the nearly 20% loss seen in some of our current systems. With the higher sensitivity, improved image quality is expected for the same patient dose. Additionally, quantitative analyses of the high count rate dynamic studies would be improved (i.e., only minimal deadtime corrections would be needed).

The performance measurements of the 400HPC camera demonstrate that the pulse tail extrapolation technique is a feasible method of addressing the problems of pulse pile-up in scintillation cameras. Our preliminary results indicate that the 400HPC does not compromise image quality at normal clinical count rates. At higher count rates the system produces better quality images than other camera systems within our clinical laboratories. It is encouraging that the capability of the nuclear medicine Anger camera can be extended without requiring elaborate or expensive changes in the basic technology.

ACKNOWLEDGMENT

The authors thank the General Electric medical systems division for its technical support. They also thank Dr. R. Kao for assistance in the early phase of data acquisition. This work was supported by National Institutes of Health Grants CA 42045 and CA 42593.

REFERENCES

1. Sorenson JA, Phelps ME. Physics in nuclear medicine. Orlando, Florida: Grune & Stratton, Inc., 1987.
2. Leo WR. Techniques for nuclear and particle physics experiments—a how-to approach. New York: Springer-Verlag, 1987.
3. Nicholson PW. Nuclear electronics. London: John Wiley & Sons, 1974.
4. Rollo FD. Nuclear medicine physics, instrumentation, and agents. St. Louis: C. V. Mosby, 1977.
5. Muehllehner G, Karp JS. A positron camera using positive-sensitive detectors: PENN-PET. *J Nucl Med* 1986; 27:90–98.
6. Performance measurements of scintillation cameras. NEMA Standards Publication NU1-1986, 1986.
7. General Electric product data and performance specifications for H3000C, DB, HF, HG, HD and HE cameras. General Electric, Milwaukee, Wisconsin.
8. Jaszczak RJ. Physical characteristics of SPECT systems, September, 1982. *J Comput Assist Tomogr* 1982; 6:1205–1215.
9. Gal R, Grenier P, Carpenter J, Schmidt DH, Port SC. High count rate first-pass radionuclide angiography using a digital gamma camera. *J Nucl Med* 1986; 27:198–206.